Adaptive guidance for low-thrust formation flight mission in Circular Relative Orbit

Acta Astronautica 234 (2025) 13–25

Contents lists available at ScienceDirect

Acta Astronautica

journal homepage: www.elsevier.com/locate/actaastro

Research paper

Adaptive guidance for low-thrust formation flight mission in Circular Relative Orbit

Dario Ruggiero [a,*], Takahiro Ito [b], Elisa Capello [a,c], Yuichi Tsuda [b]

[a] Department of Mechanical and Aerospace Engineering, Politecnico di Torino, c.so Duca degli Abruzzi 24, Turin, Torino, 10129, Italy
[b] Japan Aerospace Exploration Agency, Kanagawa, 252-5210, Japan
[c] CNR-IEIIT, Politecnico di Torino, c.so Duca degli Abruzzi 24, Turin, Torino, 10129, Italy

ARTICLE INFO

Keywords:
Formation flight
Proximity operations
Guidance algorithm
Low-thrust

ABSTRACT

Spacecraft formation flight is increasingly pivotal in the design of new space missions. This demands an high level of autonomy to optimize science time, and the development of advanced mission concepts to surpass current technological limitations. Recently, Low Earth Orbit (LEO) has been explored as solution for experimental validation of novel formation flight technologies. LEO is related to proximity formation flight missions, which require active guidance algorithms to ensure mission success and safe operations. An efficient guidance algorithm is proposed to enhance the autonomy of proximity formation flight missions, enabling variable formations and reconfiguration while ensuring safety. The optimal formation trajectory problem, conceptualized as Circular Relative Orbit, addresses the relative motion with respect to a reference orbit. Rigorous Lyapunov design is proposed to ensure convergence to the desired trajectory, guaranteeing closed-loop system stability. It incorporates an Artificial Potential Field function to deal with the formation flight problem. Initial simulations are conducted to assess the effectiveness of the proposed approach within the restricted Two-Body dynamics framework. The algorithm is applied to accomplish a space interferometer deploying mission in LEO, demonstrating its efficacy through a compact implementation. Finally, the algorithm's general and wider effectiveness is validated with elliptical and L2 Halo reference orbits.

1. Introduction

Recently, spacecraft formation flight is getting the attention of new space mission design. Having multiple spacecraft working as a single large virtual structure allows to overcome spacecraft size limitations. The main advantages of formation flight are improved flexibility and redundancy of the space mission, allowing adaptation to mission, target and number of elements, and requiring less manual intervention. Main formation flight space missions make reference to telescopes with long focal length (PROBA-3 [1], PRISMA [2], VISORS [3]) and interferometers. For what may concern space interferometers, these missions carry multiple challenges for the Guidance Navigation and Control subsystem. Generally, an interferometer mission consists of (at least) three spacecraft which are required to stay in formation with high accuracy and for long period of time. The Laser Interferometer Space Antenna (LISA) and the Deci-hertz Interferometer Gravitational Waves Observatory (DECIGO), consider three spacecraft in triangular formation for the purpose of studying and measuring gravitational waves of different frequency. Both missions requires to achieve high-accuracy formation to guarantee laser links for all the science time. These missions are more detailed in [4,5]. The Large Interferometer For Exoplanets (LIFE), details are given in [6], is another example of future five spacecraft formation flight mission design which includes the requirement of reconfiguration of the formation. In the general case, space interferometer missions select beyond-Earth orbits, where disturbances are smaller, and less intervention for formation keeping is required. Therefore, high level of autonomy must be guaranteed in order to maximize science time and/or the overall success of the mission. More details on purpose and requirements of different formation flight missions are reported in [7].

The possibility to take advantage of Low Earth Orbit (LEO) for experimental validation of new formation flight technologies is proposed in [8–10]. The reason is mainly practical and economical, but LEO formation flight opens new challenges in terms of safety and formation accuracy. Past researches on interferometer missions mainly address the autonomous attitude stabilization and control, as in [11–16]. For what may concern position, the typical approach for formation guidance is based on trajectory tracking design or leader–follower approach, as in [17–19]. This approach may be effective for interferometers with large separation distance, but LEO formation flight missions consist of

* Corresponding author.
E-mail address: dario.ruggiero@polito.it (D. Ruggiero).

https://doi.org/10.1016/j.actaastro.2025.04.026
Received 30 September 2024; Received in revised form 19 February 2025; Accepted 12 April 2025
Available online 28 April 2025

proximity maneuvers, and an active guidance is needed to guarantee safety and collision avoidance. Moreover, leader–follower approach consists of tracking the relative position with respect to the leader spacecraft, and this limits autonomy and formation reconfiguration capabilities.

In the last years, APF method has been intensely studied in space application, like in [20–22] for rendezvous and proximity maneuvers, and in [23] for gathering more spacecraft in a chosen formation. However, in both cases, the method is used to reach (and keep) a priori-known target location. This limits formation capabilities, forcing each spacecraft to reach a specified location, which is independent from the current state of the swarm (following the leader–follower approach). Lately, the concept of generalized formation approach and variable-swarm formation have been investigated using Optimal Control and Artificial Potential Field (APF). The generalized formation approach implies the spacecraft to get in a final configuration which is autonomously determined as function of the current state of the swarm. In [24], each spacecraft choose is final location following an assignment criteria between a set of target locations, while in [25,26], the formation shape and configuration is defined regulating spacecraft inter-distance and formation center. Having a generalized formation framework allows to describe each spacecraft motion with respect to a reference orbit, and without a fixed dependency with others. This framework simplifies formation adaptability to the number of elements and reconfiguration, since it is already included in the guidance algorithm design. In [25,27], Model Predictive Control is used both for guidance and control for variable-swarm formation approach. Performance and computation effort are strictly related to the definition of the prediction horizon. In [26,28], an APF function has been defined in order to attract a group of spacecraft to reach and keep the desired inter-distance. In general, in previous studies, problem statement does not comply with limitations related to actuators and fuel consumption. However, the APF method is computationally efficient, and it is possible to combine different APF function to comply with complex problem statement. Moreover, considering a realistic mission scenario includes actuators and fuel consumption constraints, leading to a final non-static configuration. For these reasons, the APF method needs to be further investigated to address guidance algorithm for non-static formation configurations, and within the generalized formation framework. Past studies on proximity formation flight do not address directly the guidance algorithm design while considering mission constraints.

This study objective is to design an effective guidance algorithm to increase the autonomy of proximity formation flight missions, allowing variable-swarm formation and reconfiguration, and guaranteeing safety. For this study, specific requirements are considered: (i) Limited actuation authority. (ii) Ability to change the spacecraft formation from a certain configuration to another. The guidance algorithm is designed under the assumption of the restricted Two-Body problem. The generalized formation framework is defined as relative motion with respect to a virtual point moving on circular orbit around the Earth. The control availability imposes tight requirements in how the spacecraft are kept in formation. First, the dynamics motion to keep a triangular formation is related with the available control input. This allows to understand how trajectory affects the required control input to keep the formation, and to identify the optimal trajectory for three (or more) spacecraft formation mission. In order to minimize the control input to keep the formation, a Circular Relative Orbit (CRO) has to be defined. Therefore, the maximum input to keep the formation is related to the main characteristics of the CRO trajectory: radius, inclination, and angular speed. This allows to relate fuel consumption to each CRO characteristic that may be changed according to mission requirements. For this study, the optimal CRO trajectory is considered. A novel guidance algorithm is designed to make the spacecraft attracted to the desired CRO trajectory. It consists of the definition of a velocity field using the Lyapunov Guidance Vector Field (LGVF) method. It is based on the work done in [29], where the problem of keeping an Unmanned Aerial Vehicle hovering over a target on a circular trajectory is addressed, and in [30–32], where it is combined with the Interfered Fluid Dynamical System method, and used for trajectory planning and collision avoidance maneuvers. The algorithm is adapted to the current problem formulation in order to generate a velocity field to track the desired CRO trajectory. The guidance formulation is augmented defining an adaptive regulation of the CRO radius. The adaptive law is based on [33], and its design guarantees the convergence and the asymptotically stability of the tracking problem of any CRO trajectory. Closed-loop system stability is guaranteed in presence of disturbances by rigorous Lyapunov analysis. Finally, the novel CRO guidance algorithm is combined with the APF function defined in [26,28] to fully address the formation flight problem. Using the proposed guidance algorithm, different proximity formation flight maneuvers are addressed in a compact implementation: formation deploying, formation keeping, formation reconfiguration. The effectiveness of the proposed guidance design is verified by means of a simulation campaign. First, the novel adaptive guidance to address CRO tracking problem is evaluated and compared with baseline LGVF-based implementation. Then, the combination with the formation function is evaluated for accurate formation flight in CRO, and in a feasible space interferometer deploying mission scenario. This mission scenario is conceptualized to test the effectiveness of the guidance algorithm for LEO applications. It consists of three main phases: (a) first spacecraft deploying in CRO trajectory, (b) second spacecraft deploying, and reaching linear formation, (c) third spacecraft deploying, and reconfiguration (triangular formation). The proposed guidance algorithm allows to address all the phases of the mission using a compact implementation.

Main studies on formation flight address elliptic reference orbits, [34–36], and beyond-Earth orbits, [37–39]. For this reason, the relevance of the proposed guidance algorithm design is emphasized considering numerical validation with different models. Elliptic reference orbits are considered to evaluate algorithm robustness and effectiveness under orbit eccentricity perturbation. L2 Halo reference orbit performance is also analyzed proving the generality of the method and its possible application in different space mission scenario. This analysis proves that, even if the guidance algorithm design is based on the restricted Two-Body problem and LEO applications, when stability conditions are satisfied, the applicability of the method is wider and more general.

The major contributions carried out in this study are: (i) The evaluation of required maximum input for formation keeping and/or reorientation for different characteristics of CRO. (ii) The design of novel adaptive guidance to address spacecraft deploying in CRO. (iii) The combination of the proposed guidance with formation flight function to address formation flight and formation reconfiguration in CRO. (iv) Theoretical design to guarantee closed-loop system convergence and asymptotically stability. The effectiveness of the proposed design is proved for a space interferometer deploying mission in LEO, and results are extended validating the performance for elliptic and L2 Halo reference orbits. Even if accuracy is not been discussed in this paper since ideal sensors are considered, the results prove the capability of the algorithm to deal with an advanced problem formulation, in terms of actuators requirements and mission feasibility, and its effectiveness for different space dynamical models.

The paper is organized as follow. In Section 2, the translational dynamics is discussed and related to the CRO definition. In Section 3, for each term contributing to the final definition of guidance algorithm, the design and the relationship to performance and stability is analyzed in detail. Simulation study and results discussion is reported in Section 4. In Section 5, the validation of the algorithm performance for elliptic and L2 Halo reference orbit is carried out by means of numerical simulations. Finally, in Section 6 conclusive remarks are given.

2. Translational dynamics

In this section, the dynamical model based on the restricted Two-Body problem is discussed and related to LEO environment. Under the assumption of circular orbit, it is possible to express the spacecraft motion using the relative position with respect to a reference frame moving on the reference orbit. Starting from this assumption, Hill's or Clohessy–Wiltshire (HCW) equations [40], are defined with respect to the origin of a Local-Vertical-Local-Horizontal (LVLH) reference frame. The LVLH reference frame is centered on the reference circular orbit of radius r_o, with x-axis oriented as the orbital velocity direction, z-axis pointing to the center of the Earth, and y-axis completing the terns. The reference object is taken as a virtual point as the origin of the LVLH frame orbiting the Earth, where the position dynamics of more spacecraft can be propagated with respect to it. The complete description of the derivation of Hill's equations from inertial equations is extensively described in [40,41], while, in the following, it is reported as the final formulation. The position dynamics is expressed as

$$\begin{cases} \ddot{x} - 2\omega\dot{z} = a_{t,x} \\ \ddot{y} + \omega^2 y = a_{t,y} \\ \ddot{z} - 3\omega^2 z + 2\omega\dot{x} = a_{t,z} \end{cases} \tag{1}$$

where $\omega = \sqrt{\mu/r_o^3}$ is the orbital angular rate, with μ as the standard gravitational parameter, $a_t = [a_{t,x},\ a_{t,y},\ a_{t,z}]^T$ is the external acceleration acting on the system. In the general case, the external acceleration is expressed as the contribution of actuators thrust (a) and external disturbances (a_d), $a_t = a + a_d$. For a formation flight mission in LEO, external disturbances are mainly related to atmospheric drag and J2 effect. In [8], typical disturbance environment is analyzed. At altitudes below 600 km and with spacecraft separation distances greater than 0.2 km, the combined effects of these disturbances can exceed magnitudes of 10^{-6} m s^{-2}. In contrast, for medium Earth orbits and high Earth orbits, the influence of atmospheric drag diminishes significantly, and perturbation effects are typically lower than 10^{-7} m s^{-2}. When focusing on proximity formations, where spacecraft separation distances are on the order of ∼0.1 km, it is crucial to account for disturbance magnitudes ranging from $10^{-6.5}$ m s^{-2} to 10^{-6} m s^{-2}. LEO presents unique challenges for formation flight missions, including shorter operational lifetimes and increased difficulty in maintaining precise control due to strong disturbances. Low-thrust electric propulsion systems, as discussed in [9], offer promising solutions for addressing the reduced lifetime issue. For this reason, this study is carried out proving system feasibility for continuous low-thrust, and assuming a maximum available acceleration of 10^{-5} m s^{-2}, chosen in compliance with the maximum disturbances acting on the system. Considering a formation of three (or more) spacecraft, it may consist of a linear or planar formation flight problem. Including the requirements of keeping the formation for long period of time (as for interferometers) limits the way the formation can be achieved. Looking at Eq. (1), it is evident that having a static triangular formation (as for interferometers) is unfeasible both for actuators thrust and fuel availability. Keeping a certain Δz and Δy, with $\dot{x} = \dot{y} = \dot{z} = 0$, requires a continuous acceleration from thrusters. In the LVLH reference frame, in order to keep the desired separation distance for long periods of time minimizing fuel consumption, each spacecraft needs to move on the same circular trajectory, which is formulated as CRO. Fig. 1 shows the trajectories of a triangular formation of three spacecraft moving on the CRO trajectory: (left) Earth Centered Reference Frame, and (right) LVLH reference frame. In the ideal case, disturbances are neglected and the acceleration is given just by the actuators thrust.

Assumption 1. Each spacecraft is moving on the same circular trajectory around the origin, and with constant angular rate $n > 0$. The general trajectory is given as

$$\begin{cases} x(t) = -\rho_x \cos(nt) \\ y(t) = \rho_y \sin(nt) \\ z(t) = \rho_z \sin(nt) \end{cases} \tag{2}$$

where $\sqrt{\rho_x^2 + \rho_y^2 + \rho_z^2} = R$, and R is the circular radius, while ρ_x, ρ_y and ρ_z denote the design parameter of the relative orbit, as in [42].

Under these assumptions, combining Eqs. (1) and (2) the acceleration required to track the desired trajectory is found as

$$\begin{cases} \cos(nt)\left[\rho_x n^2 - 2\omega n \rho_z\right] = a_x \\ \sin(nt)\left[-\rho_y n^2 + \omega^2 \rho_y\right] = a_y \\ \sin(nt)\left[-\rho_z n^2 - 3\omega^2 \rho_z + 2\omega n \rho_x\right] = a_z \end{cases} \tag{3}$$

The way the spacecraft moves on the trajectory is related to acceleration bounds expressed by

$$\begin{cases} (a_x)_{max} = |\rho_x n^2 - 2\omega n \rho_z| \\ (a_y)_{max} = |-\rho_y n^2 + \omega^2 \rho_y| \\ (a_z)_{max} = |-\rho_z n^2 - 3\omega^2 \rho_z + 2\omega n \rho_x| \end{cases} \tag{4}$$

Choosing

$$n = \omega \qquad \rho_x = R = 2\rho_z \qquad \rho_y = \sqrt{3}\rho_z \tag{5}$$

allows to have control-free circular trajectory.

Definition 1. The CRO is defined as the circular trajectory of radius R centered in the origin of the LVLH reference frame, and contained in a plane rotated around the x-axis of an angle $\phi = \pi/6$.

Remark 1. If the spacecraft is tracking the CRO trajectory with an angular rate $n = \omega$, Eq. (2) is a natural solution of Eq. (1). This implies that, in absence of external disturbances, a spacecraft moving on the CRO, stays on the CRO. Optimal CRO motion is expressed by the relationship

$$\begin{cases} \dot{x}(t) = 2\omega z(t) \\ \dot{v}(t) = -\sqrt{3}\omega x(t)/2 \\ \dot{z}(t) = -\omega x(t)/2 \end{cases} \tag{6}$$

In order to change the radius of the CRO, it is required to comply with actuators limits. An easy approach to realize this maneuver is keeping angular motion constant, $n = \omega$, and having linear radial velocity, with $\dot{\rho}_i = \beta$. This leads to a spiral trajectory expressed by

$$\begin{cases} x = -\rho\cos(nt) \\ y = \rho\cos(\phi)\sin(nt) = \frac{\sqrt{3}}{2}\rho\sin(nt) \\ z = \rho\sin(\phi)\sin(nt) = \frac{1}{2}\rho\sin(nt) \\ \dot{\rho} = \beta \end{cases} \tag{7}$$

Combining Eqs. (1) and (7) allows to define the maximum radial velocity to comply with thrusts limits, and it is given as

$$\beta \leq \frac{U}{4\omega} \tag{8}$$

where $U > 0$ is the maximum acceleration provided by the actuators. The value of β can be used to identify a convergence bound for the radial velocity. If $\dot{\rho}(t) < \beta$ for each $t > t_0$, it can be assured that thrust limit is never reached, and the closed-loop system converges to the desired CRO.

3. Guidance algorithm

In this section, guidance algorithm design is discussed. The optimal CRO trajectory tracking is expressed by Eq. (6) as velocity tracking problem. Therefore, control problem is formulated as a velocity feedback controller, given as

$$u = -K(v - v_{des}) \tag{9}$$

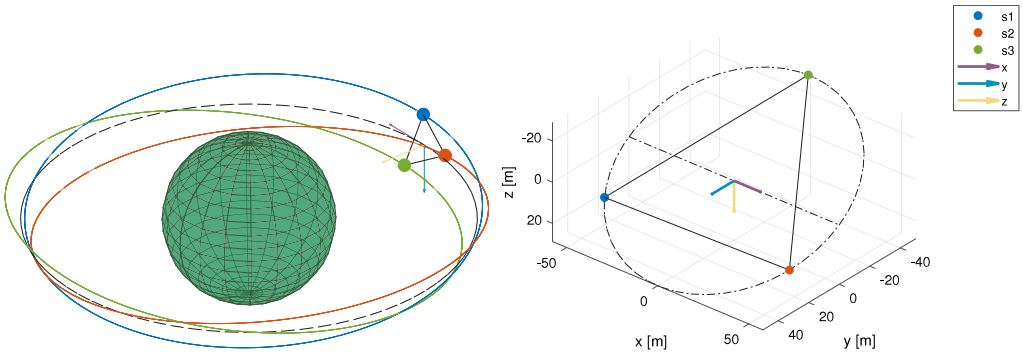

Fig. 1. Three spacecraft interferometer formation in CRO.

where $v = [\dot{x}, \dot{y}, \dot{z}]^T$ is the instantaneous velocity vector, $K \in \mathbb{R}^{3\times3}$ is diagonal gain matrix, with $K = k\mathbb{I}_3$, and v_{des} is given by the guidance algorithm. In presence of actuator constraints, the available control action is bounded by $a_i \in [-U, U]$, and given as

$$a_i = \text{sat}(u_i) = \begin{cases} U & u_i \geq U \\ u_i & -U < u_i < U \\ -U & u_i \leq -U \end{cases} \tag{10}$$

where $sat()$ is the saturation function. The guidance algorithm is designed using an APF-based approach, generating a velocity field as function of the instantaneous position of each spacecraft. The velocity field is designed as

$$v_{des} = v_{CRO} + \Delta v \tag{11}$$

and accounts for two contributions: (i) attraction to the CRO (v_{CRO}), and (ii) attraction to the formation (Δv). The spacecraft is guided along the CRO trajectory using the LGVF method, incorporating an adaptive term to ensure convergence to the desired trajectory despite actuator constraints. The formation control strategy employs an attractive–repulsive potential function to reach and maintain the desired inter-satellite separation distance. In the following, the design of each term is discussed in detail.

3.1. CRO attraction function

The CRO is defined as a circular trajectory in an inclined plane. The CRO reference frame is defined from the rotation of an angle ϕ around the x-axis of the LVLH reference frame. The rotation matrix from the CRO to the LVLH reference frame is defined as

$$Q_{CRO}^{LVLH} = \begin{bmatrix} 1 & 0 & 0 \\ 0 & \cos(\phi) & -\sin(\phi) \\ 0 & \sin(\phi) & \cos(\phi) \end{bmatrix} \tag{12}$$

The CRO attraction function is designed in the CRO reference frame, and starting from the LGVF algorithm introduced in [29,30]. Final formulation of the velocity field is expressed as

$$\begin{cases} r = \sqrt{x^{*2} + y^{*2}} \\ \delta^* = \frac{nR}{r\sqrt{(r^2+R^2)^2+\lambda(z^{*2}-H^2)^2}} \\ u^* = \delta^* \left[-x^*(r^2 - R^2) + 2y^* rR\right] \\ v^* = \delta^* \left[-y^*(r^2 - R^2) - 2x^* rR\right] \\ w^* = \delta^* \left[-\lambda r(z^* - H)\right] \end{cases} \tag{13}$$

where $p^* = [x^*,\ y^*,\ z^*]^T$ is the spacecraft position in the CRO reference frame, n and R are the CRO parameters, and $\lambda > 0$ is a constant gain. In the LVLH reference frame, the tracking velocity is given as

$$v_{CRO} = Q_{CRO}^{LVLH} \begin{bmatrix} u^* & v^* & w^* \end{bmatrix}^T \tag{14}$$

The main characteristic of the proposed guidance is that the desired velocity is normalized, and $\|v_{CRO}\|_2 = nR$. Assuming the controller to track the proposed guidance, the stability of the closed-loop system in proximity of the CRO trajectory is analyzed.

Proof. Let us consider the Lyapunov candidate function

$$V = \frac{1}{2}(v - v_{CRO})^T (v - v_{CRO}) \tag{15}$$

The closed-loop system is asymptotically stable if

$$\dot{V} = (v - v_{CRO})^T (\dot{v} - \dot{v}_{CRO}) < 0 \tag{16}$$

Considering the optimal CRO trajectory ($n = \omega$, $\phi = \pi/6$) with radius R, and assuming the spacecraft to be in proximity of the CRO, with $r \simeq R$ and $z^* \simeq H$, Eq. (13) is rewritten as

$$v_{CRO}\Big|_{r\simeq R, z^*\simeq H} = \begin{bmatrix} 2\omega z \\ -\sqrt{3}/2\omega x \\ -1/2\omega x \end{bmatrix} \tag{17}$$

In this conditions, and including actuators limitations, as control input saturation, Eq. (16) is expressed as

$$\begin{aligned} \dot{V} = &-(\dot{x} - 2\omega z)\text{sat}\left(K(\dot{x} - 2\omega z)\right) + \\ &-(\dot{y} + \sqrt{3}/2\omega x)\text{sat}\left(K(\dot{y} + \sqrt{3}/2\omega x)\right) + \\ &-(\dot{z} + 1/2\omega x)\text{sat}\left(K(\dot{z} + 1/2\omega x)\right) + \\ &+\sqrt{3}/2\omega(\dot{y} + \sqrt{3}/2\omega x)(\dot{x} - 2\omega z) - 3/2\omega(\dot{z} + 1/2\omega x)(\dot{x} - 2\omega z) \end{aligned} \tag{18}$$

where sat() is the saturation function. Considering a bounded error on the linear velocity such to have

$$\begin{cases} |\dot{x} - 2\omega z| \leq \delta \\ |\dot{y} + \sqrt{3}/2\omega x| \leq \delta \\ |\dot{z} + 1/2\omega x| \leq \delta \end{cases} \tag{19}$$

the Lyapunov function derivative is bounded by

$$\dot{V} \leq -3\delta U + \sqrt{3}/2\omega\delta^2 + 3/2\omega\delta^2 \tag{20}$$

The closed-loop system is asymptotically stable if $\dot{V} < 0$. In proximity of the CRO, the velocity error bound for guaranteeing closed-loop system stability is identified, and it is given from Eq. (20) as

$$0 \leq \delta < \frac{6U}{(3 + \sqrt{3})\omega} = \bar{\delta} \tag{21}$$

Assuming the spacecraft to be in proximity of the CRO and δ to be small such to not have control saturation, stability of the closed-loop system in presence of bounded disturbances $\|a_d\|_\infty \leq A_d$ is analyzed.

Proof. Starting from condition of Eq. (20), and assuming $K\delta < U$ and in presence of disturbances, Lyapunov function derivative is bounded by

$$\dot{V} \leq -3K\delta^2 + 3A_d\delta + \sqrt{3}/2\omega\delta^2 + 3/2\omega\delta^2. \tag{22}$$

The closed-loop system stability impose a relationship between control gain K and feedback error δ, given by

$$3K\delta^2 \geq 3A_d\delta + \frac{\sqrt{3}+3}{2}\omega\delta^2. \tag{23}$$

Eq. (23) determines the minimum value of K required to ensure closed-loop stability. Eq. (23) leads to

$$\delta\left[\left(-3K + \frac{\sqrt{3}+3}{2}\omega\right)\delta + 3A_d\right] \leq 0. \tag{24}$$

Since $\delta, A_d \geq 0$ for definition, necessary condition for Eq. (24) to admit a feasible solution is for

$$-3K + \frac{\sqrt{3}+3}{2}\omega < 0, \tag{25}$$

identifying the minimum value for the feedback gain

$$K > K_{min} = \frac{\sqrt{3}+3}{6}\omega. \tag{26}$$

In absence of external disturbances ($A_d = 0$), $K > K_{min}$ guarantees closed-loop system asymptotical stability. In presence of external disturbances ($A_d > 0$), close-loop system stability can be guaranteed for a certain value of $K > K_{min}$ for

$$\delta \geq \frac{-A_d}{-K + \frac{\sqrt{3}+3}{6}\omega}. \tag{27}$$

Including the stability condition in Eq. (21), the stability range is given by

$$\frac{-A_d}{-K + \frac{\sqrt{3}+3}{6}\omega} \leq \delta \leq \bar{\delta}. \tag{28}$$

Eq. (26) establish a theoretical minimum value of K to guarantee the existence of closed-loop system stability properties. In presence of disturbances, the minimum value of K_{min} need to guarantee the existence of Eq. (28). In this case, the minimum value of K is given as

$$K > K_{min} = \frac{A_d}{\bar{\delta}} + \frac{\sqrt{3}+3}{6}\omega. \tag{29}$$

Eq. (28) identifies the values of δ for which $\dot{V} < 0$. This implies that the closed-loop system asymptotical stability cannot be guaranteed in presence of external disturbance. However, the closed-loop system is stable and the system converge to the reference with a tracking accuracy

$$\delta(t \to \infty) \leq \frac{-A_d}{-K + \frac{\sqrt{3}+3}{6}\omega} = \rho \tag{30}$$

The choice of K influences system's responsiveness. Practical approach to choose the value of K is to guarantee a certain tracking accuracy $Tol < \bar{\delta}$. In this case, K is given as

$$K = \frac{A_d}{Tol} + \frac{\sqrt{3}+3}{6}\omega. \tag{31}$$

Remark 2. The guidance algorithm expressed by Eq. (13) addresses spacecraft attraction to CRO trajectory of radius R. Closed-loop system asymptotically stability is guaranteed in absence of disturbances ($A_d = 0$), if the initial value of δ satisfies Eq. (21), and if K satisfies Eq. (26). In the general case, with $A_d > 0$, closed-loop system stability is guaranteed if K satisfies Eq. (29), and the system converges to the reference with the tracking accuracy given in Eq. (30).

In the general case, when the spacecraft is not close to the CRO, the stability of the closed-loop system cannot be guaranteed. Due to actuators limitations, following the proposed guidance may lead to unfeasible trajectories. For this reason, the problem of getting to desired CRO is addressed as moving on an infinite number of CRO trajectories with different radius, where the instantaneous radius is changed according to an adaptive law.

Remark 3. Designing K satisfying Eq. (23) guarantees closed-loop stability along the CRO trajectory and in presence of disturbances. In the general case, disturbances may include external and internal disturbances. For the stability problem, the perturbations related to CRO radius changing and tracking the formation term Δv are considered as internal disturbances, and included in the definition of A_d.

3.2. Adaptive guidance

An adaptive law based on [33] is included to cope with actuators limitations. The adaptive law regulates the desired CRO radius R variation, from the initial value R_i to the final value R_f, according to the actual state of system. This relationship is expressed by

$$\dot{R} = \text{Proj}_{[\underline{R},\bar{R}]}\left[-Gh\left(v - v_{ref}\right) - \gamma\left(R - R_f\right)\right] \tag{32}$$

where $\underline{R} \leq \min(R_i, R_t)$ and $\bar{R} \geq \max(R_i, R_t)$, and $G, \gamma > 0$ are constant gains. The function $h = h(x)$ gives the element x_i of the vector x which satisfy $|x_i| = \|x\|_\infty$. Considering the spacecraft motion from R_i to R_f with $R_f > R_i$, in order to comply with the stability condition given in Eq. (21), the radius is increased when

$$\dot{R} > 0 \qquad \text{if} \qquad \max\left(\left|v - v_{ref}\right|\right) < \eta\bar{\delta} \tag{33}$$

with $0 < \eta < 1$. and it leads to

$$0 < -G\eta\bar{\delta} - \gamma(R - R_f) \leq -G\eta\bar{\delta} - \gamma(\underline{R} - \bar{R}) \tag{34}$$

This consideration allows to design G guaranteeing stability during radius increasing, and it is given as

$$G \geq \gamma\frac{\bar{R} - \underline{R}}{\eta\bar{\delta}} \tag{35}$$

Similar consideration is done for the definition of γ using the condition expressed in Eq. (8) for control input saturation. It is given as

$$\dot{R} \leq \gamma\left[-\frac{\bar{R} - \underline{R}}{\eta\bar{\delta}}\delta - (\underline{R} - \bar{R})\right] \leq \gamma(\bar{R} - \underline{R}) \leq \beta \quad \rightarrow \quad \gamma \leq \frac{\beta}{\bar{R} - \underline{R}} \tag{36}$$

Remark 4. The proposed guidance algorithm, combining Eqs. (13) and (32), allows to make the closed-loop system converge to desired CRO trajectory. Assuming the spacecraft being in proximity of a feasible CRO trajectory which is related to the initial conditions (with radius R_i), and with the initial velocity error satisfying Eq. (21), following the proposed guidance, the spacecraft reach autonomously the desired CRO with radius R_f. If the adaptive law gains are designed according to Eqs. (35) and (36), the stability of the closed-loop system for each $R \in [R_i, R_f]$ is guaranteed, and the control input is within the saturation bounds. Same conditions hold for $R_i > R_f$.

In practice, the maximum $\dot{R}$ value is related to $R = \underline{R}$ and $\delta = 0$. Therefore, the design proposed in Eq. (36) is really conservative, and it leads to long maneuvering times. Time-performance trade off is achieved considering an intermediate design condition, $\delta = \epsilon\bar{\delta}$. It is expressed by

$$\dot{R} \leq \gamma^*\left[-\frac{\bar{R} - \underline{R}}{\eta\bar{\delta}}\epsilon\bar{\delta} + (\bar{R} - \underline{R})\right] = \gamma^*(\bar{R} - \underline{R})(1 - \epsilon/\eta) \leq \beta \tag{37}$$

which leads to

$$\gamma \leq \gamma^* \leq \frac{\beta}{(\bar{R} - \underline{R})(1 - \epsilon/\eta)} \tag{38}$$

with $0 \leq \epsilon < \eta$. Closer is ϵ/η to 1, higher is the possibility to have the controller operating in proximity of the saturation bounds.

3.3. Formation attraction function

The guidance function attracting the spacecraft to formation is expressed by two main contributions. First, the swarm gathering is addressed using the equilibrium shaping method, introduced in [26,28]. This leads to the definition of an attractive–repulsive function with the purpose to reach the desired distance between the spacecraft. For the ith spacecraft, it is expressed starting from the potential function

$$E_{gath,i} = \sum_{j\neq i}^{N-1} \frac{a}{2} x_{ij}^T x_{ij} + \frac{cb}{2} e^{-\frac{x_{ij}^T x_{ij}}{c}} \tag{39}$$

where $x_{ij} \in \mathbb{R}^3$ is the relative position vector pointing from ith to jth spacecraft, and $a, b, c > 0$ are constant gains. In particular, a is defined as

$$a = be^{-\frac{d^2}{c}} \tag{40}$$

where $d \in \mathbb{R}$ is the desired separation distance. Following the APF approach, the potential field defined in Eq. (39) is used to define the velocity field

$$\Delta v_i = -\nabla E_{gath} = -\sum_{j\neq i}^{N-1} x_{ij} b \left(e^{-\frac{d^2}{c}} - e^{-\frac{x_{ij}^T x_{ij}}{c}} \right) \tag{41}$$

that goes to 0 when $x_{ij}^T x_{ij} = d^2$. Tracking the velocity field makes the spacecraft reach the desired separation distance. Gain design is based on the characterization of the function for the one dimensional (1D) case. The linearization around the origin of Eq. (41) leads to

$$x \to 0 \qquad \Delta v_i \simeq b \left(1 - e^{-\frac{d^2}{c}} \right) x \tag{42}$$

Considering the limitation of the linearized function in the interval $x \in [-d/2, d/2]$, it is possible to design b such to have

$$|\Delta v_i| \leq \alpha\bar{\delta} \qquad \rightarrow \qquad b \leq \frac{\alpha\bar{\delta}}{\left(1 - e^{-\frac{d^2}{c}} \right) d/2} \tag{43}$$

The design of c is based on the qualitative representation of Eq. (41) for the 1D case, Fig. 2, where b is designed according to Eq. (43). In practice, the application of this approach in the considered problem leads to long settling time. Settling time performance of the formation attraction term are improved augmenting Eq. (41) with a term based on formation mean position. It is designed using an attractive-parabolic APF function given as

$$E_{att} = \frac{1}{2} k_{att} \sum_{j=1}^{N} \frac{x_j^T x_j}{N} \tag{44}$$

where $k_{att} > 0$ is an attractive gain, x_j is the position of the jth spacecraft, and N is the number of spacecraft in formation. The final formulation of the formation attraction velocity field for the ith spacecraft is given as

$$\Delta v_i = -\nabla(E_{gath,i} + E_{att}) = -\sum_{j\neq i}^{N-1} x_{ij} b \left(e^{-\frac{d^2}{c}} - e^{-\frac{x_{ij}^T x_{ij}}{c}} \right) - k_{att} \sum_{j=1}^{N} \frac{x_j}{N} \tag{45}$$

As discussed in the previous sections, the condition to guarantee the stability of the closed-loop system is tight due to the actuators limitations. Moreover, moving outside of the optimal CRO trajectory increase significantly fuel consumption. In order to limit the effect of the formation attraction function, Eq. (45) is evaluated considering jth spacecraft in-plane projection on the current ith spacecraft CRO trajectory. This is shown in Fig. 3, where the dots denote the projection. In this case, the desired separation distance d is not constant, but it is changed with R as

$$d = \begin{cases} 2R & \text{with } N = 2 \\ R\sqrt{3} & \text{with } N = 3 \end{cases} \tag{46}$$

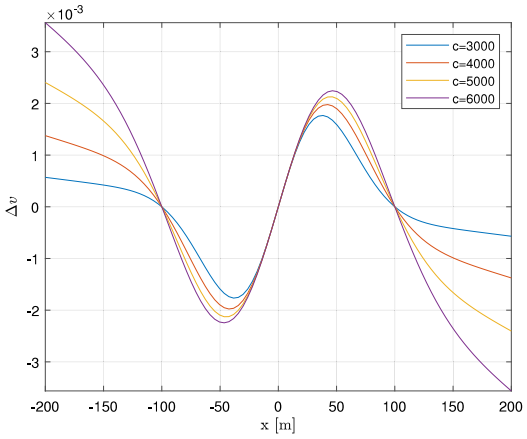

Fig. 2. 1D formation attraction function.

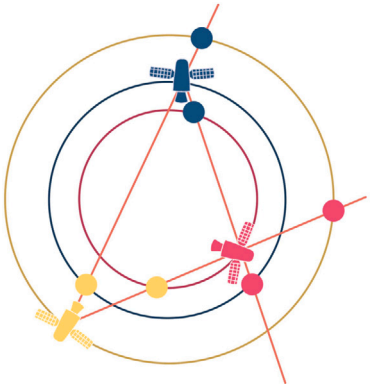

Fig. 3. Spacecraft projection on CRO.

In this way, when the spacecraft is on the desired CRO, the effect of dragging it out of its trajectory is reduced, and the formation gathering maneuver results to be similar to a re-phasing maneuver on the CRO trajectory.

4. Numerical simulations for LEO two-body problem

In this section, simulation study is carried out to evaluate the effectiveness and the performance of the proposed approach. Considering the Two-Body dynamics, Eq. (1), a novel guidance algorithm for formation flight mission is designed in order to guarantee closed-loop system convergence and asymptotically stability to CRO trajectory. The guidance algorithm is summarized in Algorithm 1. First, the attraction of a single spacecraft to the desired CRO trajectory is evaluated. This is achieved combining LGVF, Eq. (13), with an adaptive law, Eq. (32), to regulate CRO radius increasing. Then, the guidance function is augmented with Eq. (45) to address formation flight problem. Simulation study is divided in three main parts: (i) single spacecraft tracking the CRO trajectory. (ii) three spacecraft formation in proximity of the desired CRO. (iii) Interferometer deploying mission scenario.

The first simulation scenario consists of single spacecraft deploying in different CROs. Fig. 4 shows spacecraft trajectories considering different CRO's radius R_f. It is observed a limit in the application of LGVF guidance, Eq. (13), which leads to closed-loop system instability. The inclusion of the adaptive radius, Eq. (32), overcomes this limitation increasing the applicability of the proposed approach. Moreover, maximum values of δ are reported in Table 1. The proposed approach reduces significantly the value of δ. For the LGVF ($R = 50$ m) case, even if δ_{max} exceed $\bar{\delta} = 15.4$ mm s^{-1}, the closed-loop system is converging

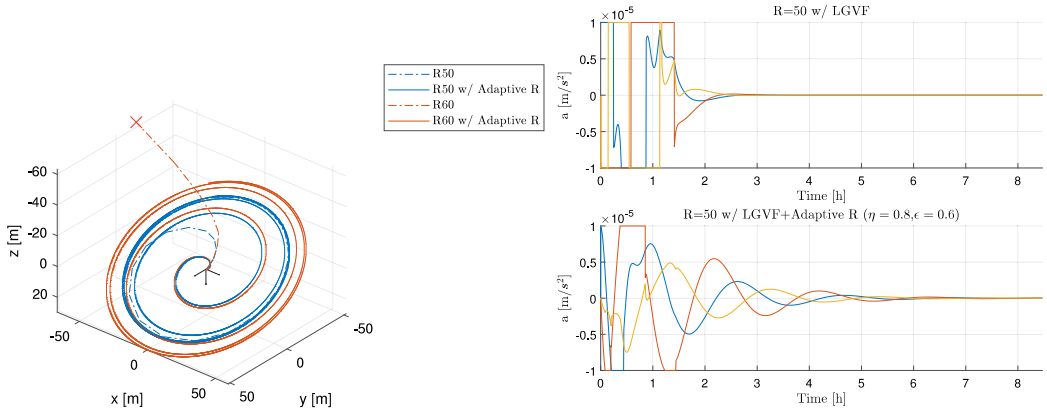

Fig. 4. Comparison with the inclusion of the adaptive term.

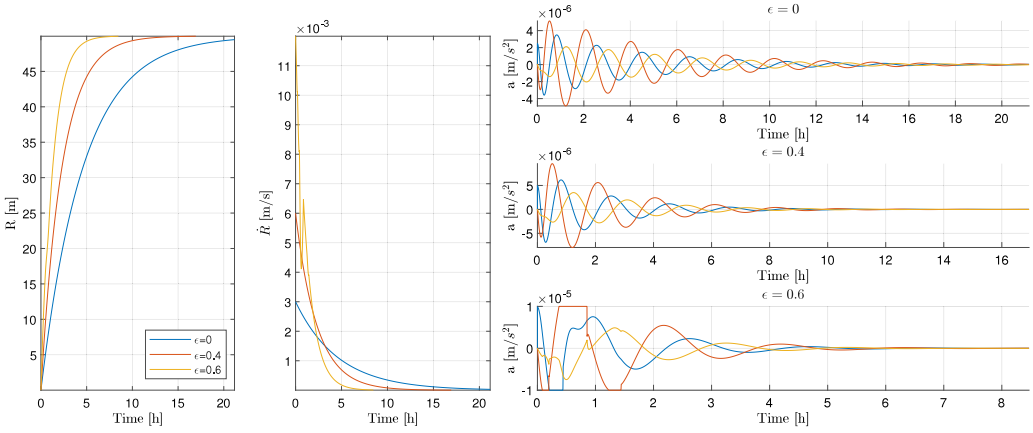

Fig. 5. Deploying in CRO with $R = 50$ m: Closed-loop system performance for different values of ϵ.

Algorithm 1: Adaptive LGVF for formation flight in CRO

Data: p, v, p_{ij}, R
Result: $a, \dot{R}$
Update:
  $v_{CRO} \leftarrow v_{CRO}(p, R)$; /* Equations (13)-(14) */
  $\Delta v \leftarrow \Delta v(p_{ij})$; /* Equation (45) */
  $v_{des} \leftarrow v_{CRO} + \Delta v$;
  $\dot{R} \leftarrow \dot{R}(v, v_{des}, R, R_f)$; /* Equation (32) */
Compute:
$u \leftarrow -K(v - v_{des})$;
$a \leftarrow$sat(u) is applied to the spacecraft;

to desired value. This implies that stability condition given in Eq. (21) is conservative. The proposed approach leads to longer maneuvering time, but control input is smoother, and this behavior is preferred for continuous thrusters. The effect of ϵ is shown in Fig. 5. Closer is ϵ/η to 1, more reactive is the guidance. This allows to reduce the time required to complete the maneuver, but the control input is higher, and may reach saturation bounds more often.

Control and guidance algorithms' parameters are summarized in Table 2. For the considered parameters, convergence radius expressed in Eq. (30) is $\rho = 0.19$ μm s^{-1}, while in simulation tracking accuracy is 0.10 μm s^{-1}. In Fig. 6, the performance of the combination of the CRO guidance and the formation term are shown. A triangular formation of three spacecraft with $d = 100$ m separation distance is considered. Each spacecraft is assumed to be in proximity of the CRO with an error of the order of magnitude of m for position and mm s^{-1} for velocity. Formation accuracy is not discussed because ideal sensors are considered, and the formation parameters converge to desired value in reasonable time.

Table 1
Maximum δ for single spacecraft deploying in CRO.

Guidance (CRO radius)	δ_{max} [mm s^{-1}]
LVGF ($R = 50$ m)	41.2
LVGF ($R = 60$ m)	∞
LVGF + Adaptive R ($R_f = 50$ m, $\epsilon = 0$)	0.0714
LVGF + Adaptive R ($R_f = 50$ m, $\epsilon = 0.4$)	0.0761
LVGF + Adaptive R ($R_f = 50$ m, $\epsilon = 0.6$)	3.40
LVGF + Adaptive R ($R_f = 60$ m, $\epsilon = 0.6$)	3.90

Finally, a possible autonomous interferometer deploying mission is considered. It consists of three main phases: (i) first spacecraft deployment in CRO (ii) second spacecraft deployment, and linear formation (iii) third spacecraft deployment, and triangular formation. Initial condition is set as x-direction release, and it is expressed as

$$x_1 = \begin{bmatrix}\Delta x & 0 & 0\end{bmatrix}^T \qquad x_2 = \begin{bmatrix}-\Delta x & 0 & 0\end{bmatrix}^T \qquad x_3 = \begin{bmatrix}0 & 0 & 0\end{bmatrix}^T \tag{47}$$

and $v_i = [0,\ 0,\ 0]^T$ with $i = 1, 2, 3$. Fig. 7 shows spacecraft trajectories for each mission phase, and in Fig. 8 time variation of the main data is reported. The results show that the proposed design is able to comply with all the phases of the mission in a compact implementation, dealing both with linear and triangular formation in CRO.

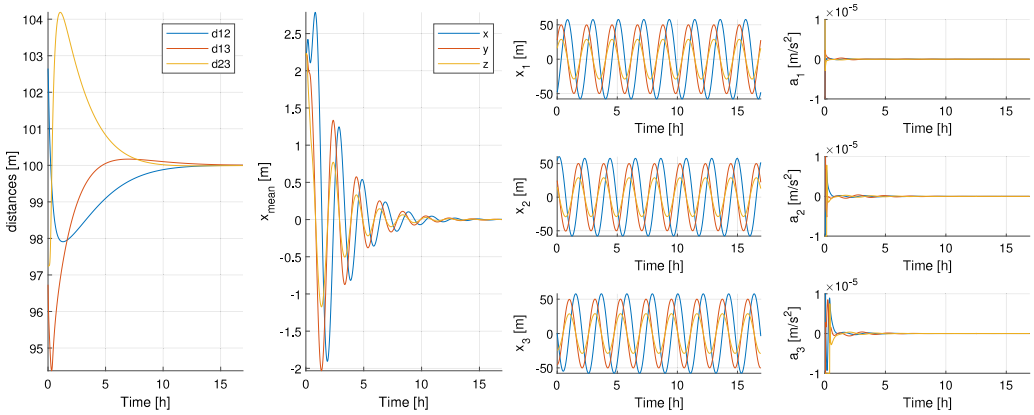

Fig. 6. Formation keeping: Positions and control inputs.

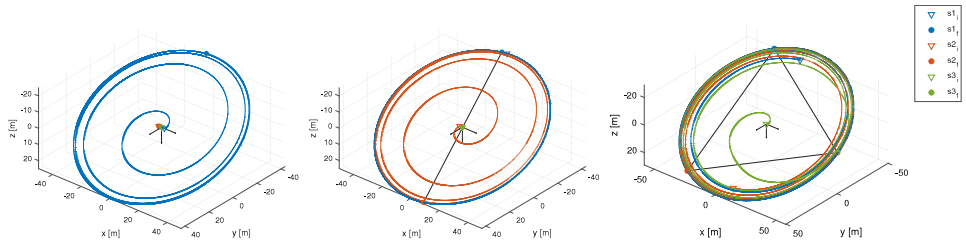

Fig. 7. Trajectories for 3-phases formation deploying mission in LEO.

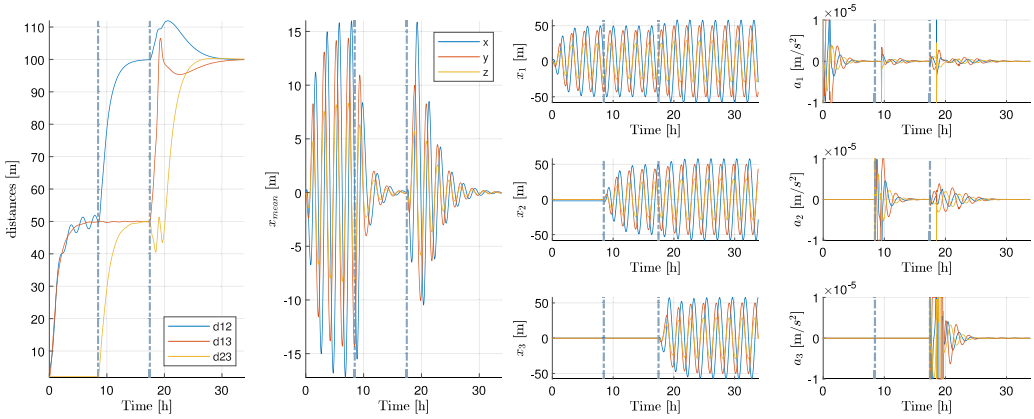

Fig. 8. Formation deploying mission in LEO: Positions and control inputs.

Table 2
Guidance and control parameters.

Parameter	Value	Parameter	Value
K	10	α	0.25
η	0.8	c	5000
ϵ	0.6	b	8.90×10^{-5}
γ	2.08×10^{-4}	k_{att}	1.66×10^{-4}
G	0.97	U	10×10^{-6}
r_o	8378 [km]	A_d	$10^{-6.5}$

5. Numerical simulations with different models

In this section, the results presented for the Two-Body problem are extended considering algorithm performance validation with different dynamical models. First, the effects of Earth orbit eccentricity is evaluated considering Tschauner–Hempel (TH) model. Then, Three-Body problem is addressed considering motion around the Earth–Moon second Lagrangian point (L2).

5.1. Elliptical reference orbit

For a highly elliptical reference orbit, HCW Equations are not valid. Alternative models have been developed dealing with orbit eccentricity $0 < e < 1$. TH model provides a linear time varying model for proximity relative motion on elliptic orbits. As shown in [43–45], typical approach is to consider the target true anomaly ν_T as an independent variable. The linearized TH model is given as

$$\begin{cases} \ddot{x} = (\omega_T^2 - \omega^2)x + 2\omega_T \dot{z} - \gamma_T z + a_x \\ \ddot{y} = -\omega^2 y + a_y \\ \ddot{z} = (\omega_T^2 + 2\omega^2)z - 2\omega_T \dot{x} + \gamma_T x + a_z \end{cases} \tag{48}$$

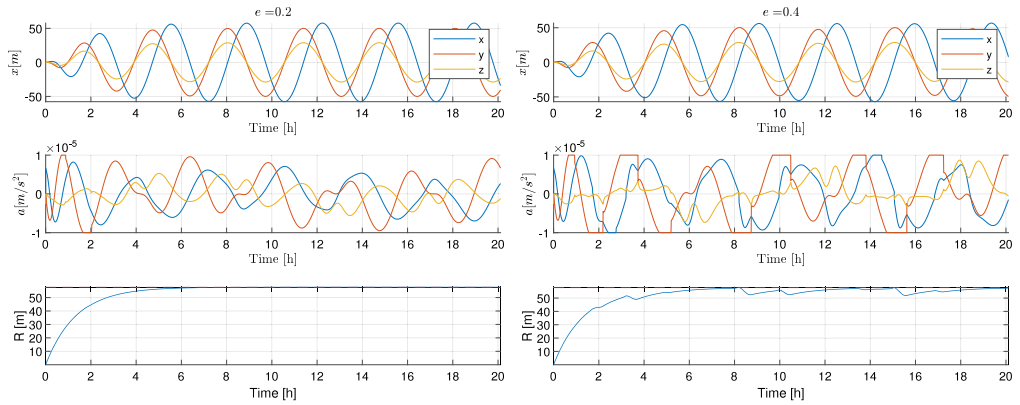

Fig. 9. CRO tracking for Elliptic reference orbit with ($a_o = 17\,056$ km, $e = 0.2$) and ($a_o = 26\,532$ km, $e = 0.4$).

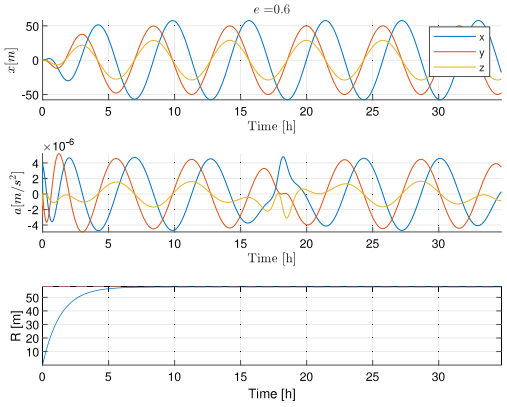

Fig. 10. CRO tracking for Elliptic reference orbit with $a_o = 65\,484$ km and $e = 0.6$.

where ω_T is time derivative of ν_T, and it is defined as

$$\omega_T = \frac{\sqrt{\mu a_o(1-e^2)}}{r_T^2} \tag{49}$$

with a_o as the major semi-axis, and r_T is the target instantaneous radius, with

$$r_T = \frac{a_o(1-e^2)}{1+e\cos\nu_T} \tag{50}$$

and $\omega = \sqrt{\mu/r_T^3}$. The parameter γ_T is the second time derivative of target true anomaly, and it is given by

$$\gamma_T = -\frac{2\mu e \sin\nu_T}{r_T^3} \tag{51}$$

The reference frame is defined as the LVLH reference frame centered on a virtual point moving on the reference elliptical orbit. It is defined with z-axis pointing to the main body, y-axis parallel to the orbit angular momentum, and x-axis completing the right-handed set.

The TH model, Eq. (48), can be traced back to HCW model, Eq. (1), where the following terms are included as disturbances

$$\begin{cases} a_{e,x} = (\omega_T^2 - \omega^2)x + 2(\omega_T - \omega)\dot{z} - \gamma_T z \\ a_{e,y} = 0 \\ a_{e,z} = (\omega_T^2 - \omega^2)z - 2(\omega_T - \omega)\dot{x} + \gamma_T x \end{cases} \tag{52}$$

Orbital disturbances related to eccentricity are bounded between apogee and perigee, with

$$a_e(r_T = r_a) = \underline{a_e} \le a_e \le \bar{a}_e = a_e(r_T = r_p) \tag{53}$$

Considering the spacecraft moving on the CRO trajectory from Eq. (2) with $n = \bar{\omega} = \omega(r_t = r_p)$, perturbation bounds can be determined as

$$r_T = r_p \rightarrow \begin{cases} \bar{a}_{e,x} = (\bar{\omega}_T\bar{\omega} - \bar{\omega}_T^2)R\cos(\bar{\omega}t) - \bar{\gamma}_T\frac{R}{2}\sin(\bar{\omega}t) \\ \bar{a}_{e,y} = 0 \\ \bar{a}_{e,z} = (\bar{\omega}_T^2 - 4\bar{\omega}_T\bar{\omega} + 3\bar{\omega}_T^2)\frac{R}{2}\sin(\bar{\omega}t) - \bar{\gamma}_T R\cos(\bar{\omega}t) \end{cases} \tag{54}$$

However, moving with $n = \bar{\omega}$ in proximity of the apogee (where $\omega = \underline{\omega}$) introduce an additional perturbation, which is related to the CRO tracking with different angular velocity, and expressed in Eq. (3). Therefore, in the apogee the total orbital perturbation acting on the spacecraft is

$$a_{e,t}(r = r_a) = \underline{a_e} + \begin{bmatrix} R\cos(\bar{\omega}t)(\bar{\omega}^2 - \bar{\omega}\underline{\omega}) \\ \frac{\sqrt{3}}{2}R\sin(\bar{\omega}t)(-\bar{\omega}^2 + \underline{\omega}^2) \\ \frac{R}{2}\sin(\bar{\omega}t)(-\bar{\omega}^2 - 3\underline{\omega}^2 + 4\underline{\omega}\bar{\omega}) \end{bmatrix} \tag{55}$$

while $a_{e,t}(r = r_p) = \bar{a}_e < a_{e,t}(r = r_a)$. Perturbation term related to orbit eccentricity is bounded, satisfying the first assumption for the stability condition. Therefore, if the perturbation terms do not exceed the available control input, and if Eq. (23) is satisfied, closed-loop system stability is guaranteed, and the tracking error converges to the convergence radius ρ, defined in Eq. (30).

CRO trajectory tracking performance are evaluated in relationship with the perturbation introduced by the elliptic orbit (with orbit inclination $i = 0$). In Figs. 9 and 10, the effect of the perturbation is shown. Having a low orbit formation is not compatible with high eccentricity, because the perturbation exceeds actuator bounds. Indeed, in Fig. 9, the system successfully tracks the desired CRO trajectory for $e = 0.2$. However, for $e = 0.4$, the actuators are unable to fully counteract the time-varying orbital perturbations. In this scenario, the proposed algorithm dynamically adapts the CRO radius, preventing the closed-loop system from becoming unstable. The bottom plot illustrates the time variation of the trajectory radius R, which decreases in response to the thruster acceleration reaching its saturation limit, ensuring controllability despite actuator constraints. This is possible because the perturbations effect is limited, and does not drive the system to $\delta > \bar{\delta}$. In case of a larger perturbation, tracking error may exceed $\bar{\delta}$ leading the system to critical instability. Considering high Earth orbit allows to track the CRO trajectory also in case of high eccentricity. For the considered examples, the maximum perturbation related to model error D_m is related to convergence radius ρ, and values are reported in Table 3. Finally, in Fig. 11, formation performance are evaluated considering High-Earth orbit with high eccentricity. In particular, this simulation scenario considers three spacecraft getting in triangular formation starting from the initial condition of Eq. (47). Results confirm the capability of the algorithm to cope with perturbations, while satisfying formation and collision avoidance requirements.

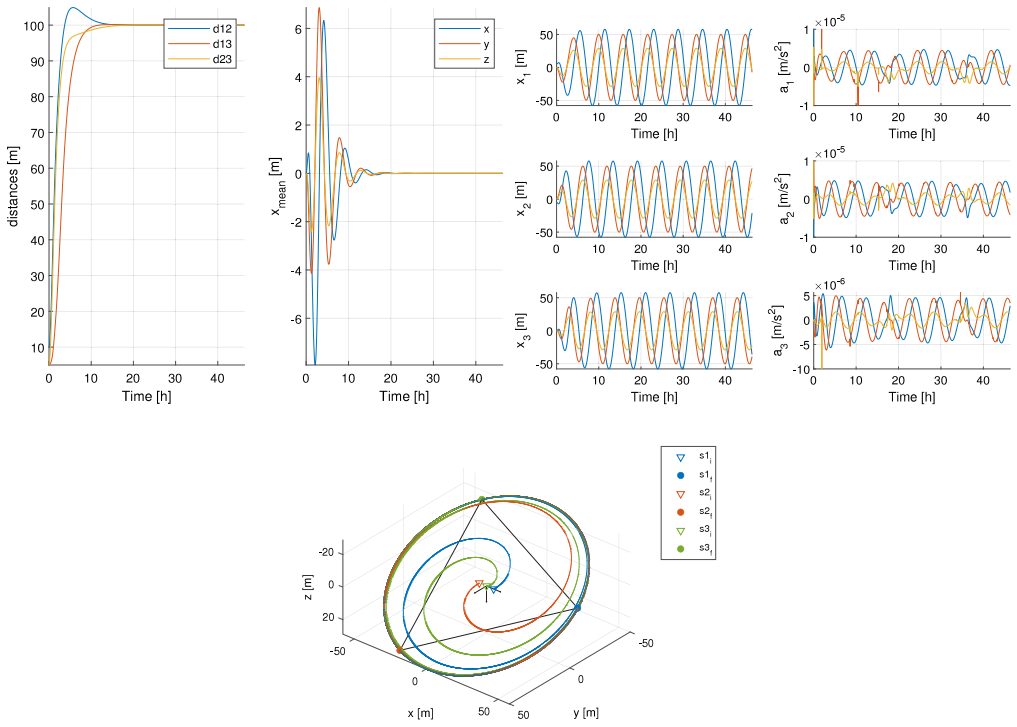

Fig. 11. Triangular formation in CRO for Elliptic reference orbit with $a_o = 65\,484$ km and $e = 0.6$.

Table 3
Convergence accuracy and maximum tracking error for Elliptic reference orbit.

Reference orbit (Semi-axis, Eccentricity)	δ_{max} [mm s^{-1}]	D_m [μm s^{-2}]	ρ [μm s^{-1}]	$\delta(t \to \infty)$ [μm s^{-1}]
$a_o = 17\,056$ km, $e = 0.2$	0.4	6.5	1.0	0.10
$a_o = 26\,532$ km, $e = 0.4$	6	13	–	–
$a_o = 65\,484$ km, $e = 0.6$	0.00006	7.7	0.5	0.06

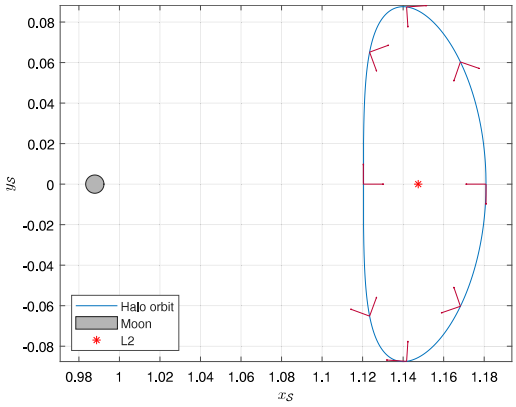

Fig. 12. L2 Halo reference orbit.

5.2. Restricted three-body dynamics

The Three-body Problem, as in [46], consists of relating the position of a small body (with mass m_3) with two primaries (m_1 and m_2). The mass is restricted such that $m_1 > m_2 \gg m_3$. In addition, and assuming the motion of m_2 with respect to m_1 to be circular, the motion of m_1 and m_2 is Keplerian. Therefore, the motion of m_3 is described considering the rotating reference frame $\mathcal{S}$ centered in the center of mass. The axes are defined with x_S pointing toward m_2, z_S parallel to the angular velocity vector related to the Keplerian primary orbits, and y_S completing the right-handed set. The equation of motion is generalized introducing characteristic values

$$L^* = \|R_1\|_2 + \|R_2\|_2, \qquad m^* = m_1 + m_2, \qquad t^* = \sqrt{\frac{L^{*3}}{G_c m^*}} \tag{56}$$

where R_i is the position of the primaries in the reference frame $\mathcal{S}$, and G_c is the universal gravitational constant. In this way, the equation of motion in the reference frame $\mathcal{S}$ is defined by means of dimensionless quantities, and, as in [37], it is given by

$$\begin{cases} \ddot{x}_S = 2\dot{y}_S + x_S - \frac{(1-\mu)(x_S+\mu)}{r_{13}^3} - \frac{\mu(x_S-1+\mu)}{r_{23}^3} + a_{S,x} \\ \ddot{y}_S = -2\dot{x}_S + y_S - \frac{1-\mu}{r_{13}^3} y_S - \frac{\mu}{r_{23}^3} y_S + a_{S,y} \\ \ddot{z}_S = -\frac{1-\mu}{r_{13}^3} z_S - \frac{\mu}{r_{23}^3} z_S + a_{S,z} \end{cases} \tag{57}$$

where $p_S = [x_S,\ y_S,\ z_S]^T$ is the spacecraft position in $\mathcal{S}$ reference frame, the dimensionless time derivative is computed with respect to $\tau = t/t^*$, $\mu = m_2/m^*$ is the mass ratio, and r_{13} and r_{23} are dimensionless relative distance with respect to the two primaries, and defined as

$$r_{13} = \sqrt{(x_S+\mu)^2 + y_S^2 + z_S^2}, \qquad r_{23} = \sqrt{(x_S-1+\mu)^2 + y_S^2 + z_S^2} \tag{58}$$

Reference orbit p_S^0 (Fig. 12) is selected as Earth–Moon L2 Halo orbit, and it is defined considering free motion ($a_S = 0$) and the initial condition provided in [47]. So, as in [38,39,48,49], the spacecraft motion is described by the relative position p' with respect to a virtual point moving as the reference trajectory p_S^0. The spacecraft position is given as

$$p_S = p_S^0 + p' \tag{59}$$

Assuming the spacecraft to move in proximity of the reference orbit, and p' to be small with respect to p_S^0, the relative position $p' = [x',\ y',\ z']^T = p_S - p_S^0$ is expressed as

$$\begin{cases} \ddot{x}'_S = 2\dot{y}'_S + x'_S - \frac{1-\mu}{r_{13}^3} x'_S - \frac{\mu}{r_{23}^3} x'_S + a_{S,x} \\ \ddot{y}'_S = -2\dot{x}'_S + y'_S - \frac{1-\mu}{r_{13}^3} y'_S - \frac{\mu}{r_{23}^3} y'_S + a_{S,y} \\ \ddot{z}'_S = -\frac{1-\mu}{r_{13}^3} z'_S - \frac{\mu}{r_{23}^3} z'_S + a_{S,z} \end{cases} \tag{60}$$

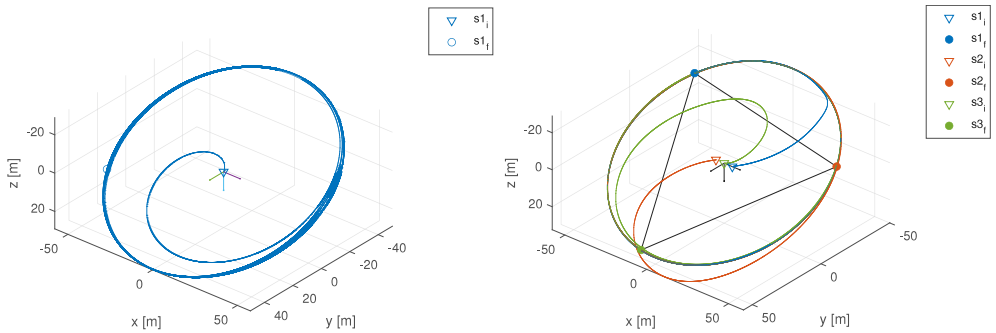

Fig. 13. Relative trajectories: (**left**) Single spacecraft trajectory (**right**) Triangular formation in CRO.

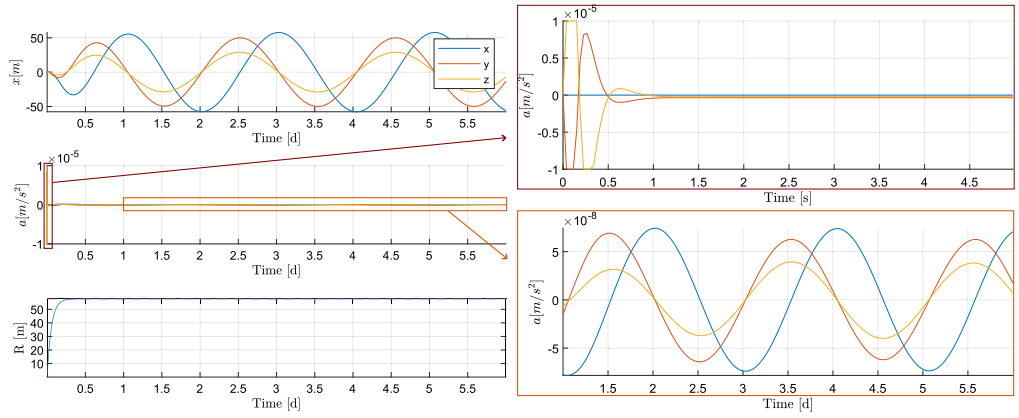

Fig. 14. CRO tracking for L2 Halo reference orbit (**left**). Zoom on actuators thrust for the initial acceleration, and steady state orbital disturbances compensation (**right**).

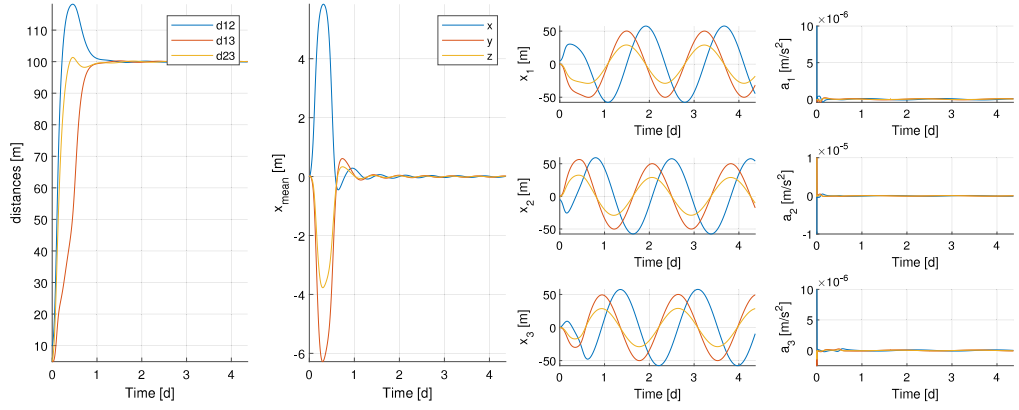

Fig. 15. Triangular formation in CRO for L2 Halo reference orbit.

where $r_{13} \simeq r_{13}^0$ and $r_{23} \simeq r_{23}^0$. The relative motion is expressed in the LVLH reference frame considering the z-axis pointing to L2, y-axis parallel to the orbit angular momentum, and x-axis completing the right-handed set. LVLH reference frame is reported along with the L2 Halo trajectory for different values of p^0 in Fig. 12.

Relative trajectories in the LVLH reference frame are reported in Fig. 13, for a single spacecraft tracking the CRO trajectory, and for the triangular formation scenario. In Fig. 14, CRO tracking performance for a single spacecraft motion with respect to Halo reference orbit are evaluated. Thrusters acceleration is zoomed, highlighting the difference between the initial acceleration, and the steady-state action to counteract orbital perturbations. The algorithm is effective and it allows to reach the CRO trajectory in short time. It is tracked for all the orbital period. Residual acceleration to stay on the CRO trajectory is affected by the CRO angular speed n and inclination ϕ. The values of n and ϕ are not optimized for this problem, because it is out of the purpose of this study. However, model error is evaluated in simulation and in comparison with HCW model, considering CRO tracking velocity $n = 0.035$ mrad s^{-1}, and $\omega = n$. Maximum perturbation during CRO tracking related to model error is $D_m = 0.15$ μm s^{-2}, which corresponds to convergence radius $\rho = 0.015$ μm s^{-1}. Maximum tracking error is $\delta_{max} = 0.02$ mm s^{-1}, and the CRO tracking accuracy is 0.008 μm s^{-1}. Formation flight performance are evaluated in Fig. 15, and considering the simultaneous release of three spacecraft starting from the initial conditions given in Eq. (47). Spacecraft gets in triangular formation in

short time. Results confirm the generality of the algorithm, proving that its application can be extended to different dynamics.

6. Conclusions

Recent studies have proposed the possibility to take advantage of LEO for improvement and validation of new formation flight technologies. Considering LEO environment and limited thrust leads to proximity operations formation flight problem, which requires an active guidance algorithm to guarantee mission success and safe operations. In this context, the design of an autonomous guidance approach for formation flight mission in LEO is addressed. Formation keeping of three (or more) spacecraft for long periods of time, while minimizing fuel consumption, is formulated as CRO trajectory tracking problem. A novel guidance algorithm based on LGVF is designed to deal with formation flight problem in CRO. The convergence of the spacecraft trajectory to the CRO and closed-loop system stability is guaranteed by the design of an adaptive term. This guidance algorithm is combined with an APF function to address the formation flight problem. Simulation study is carried out to evaluate the performance of the proposed approach. First, convergence and stability of the closed-loop system are verified for the CRO trajectory tracking problem. Then, the combination with formation flight problem is addressed. Low-thrust space interferometer deploying mission scenario is conceptualized to evaluate the performance of the algorithm for different mission phases. The considered mission scenario consists of three main phases: (a) first spacecraft deploying in CRO trajectory, (b) second spacecraft deploying, and reaching linear formation, (c) third spacecraft deploying, and reconfiguration (triangular formation). The proposed guidance algorithm allows to address all the phases of the mission using a compact implementation. Moreover, the relevance of the proposed approach is emphasized considering the application in different space scenarios. Numerical simulation are carried out to verify guidance algorithm effectiveness for elliptical orbits and Earth–Moon L2 Halo orbit. Accuracy has not been discussed in this paper since ideal sensors are considered. However, the results prove the feasibility to deal with an advanced problem formulation, in terms of actuators requirements and mission feasibility.

CRediT authorship contribution statement

Dario Ruggiero: Writing – review & editing, Writing – original draft, Visualization, Validation, Methodology, Investigation, Formal analysis, Data curation, Conceptualization. **Takahiro Ito:** Writing – review & editing, Writing – original draft, Supervision, Investigation, Formal analysis, Conceptualization. **Elisa Capello:** Writing – review & editing, Writing – original draft, Supervision, Methodology, Formal analysis, Conceptualization. **Yuichi Tsuda:** Writing – review & editing, Writing – original draft, Supervision, Formal analysis, Conceptualization.

Declaration of competing interest

The authors declare that they have no known competing financial interests or personal relationships that could have appeared to influence the work reported in this paper.

References

[1] J.S. Llorente, A. Agenjo, C. Carrascosa, C. de Negueruela, A. Mestreau-Garreau, A. Cropp, A. Santovincenzo, PROBA-3: Precise formation flying demonstration mission, Acta Astronaut. 82 (1) (2013) 38–46.

[2] S. D'Amico, P. Bodin, M. Delpech, R. Noteborn, Prisma, in: Distributed Space Missions for Earth System Monitoring, Springer, 2012, pp. 599–637.

[3] A. Koenig, S. D'Amico, E.G. Lightsey, Formation flying orbit and control concept for the visors mission, in: AIAA Scitech 2021 Forum, 2021, p. 0423.

[4] P. Amaro-Seoane, H. Audley, S. Babak, J. Baker, E. Barausse, P. Bender, E. Berti, P. Binetruy, M. Born, D. Bortoluzzi, et al., Laser interferometer space antenna, 2017, arXiv preprint arXiv:1702.00786.

[5] S. Kawamura, M. Ando, N. Seto, S. Sato, M. Musha, I. Kawano, J. Yokoyama, T. Tanaka, K. Ioka, T. Akutsu, et al., Current status of space gravitational wave antenna DECIGO and B-DECIGO, Prog. Theor. Exp. Phys. 2021 (5) (2021) 05A105.

[6] S.P. Quanz, M. Ottiger, E. Fontanet, J. Kammerer, F. Menti, F. Dannert, A. Gheorghe, O. Absil, V.S. Airapetian, E. Alei, et al., Large interferometer for exoplanets (LIFE)-I. Improved exoplanet detection yield estimates for a large mid-infrared space-interferometer mission, Astron. Astrophys. 664 (2022) A21.

[7] G. Di Mauro, M. Lawn, R. Bevilacqua, Survey on guidance navigation and control requirements for spacecraft formation-flying missions, J. Guid. Control Dyn. 41 (3) (2018) 581–602.

[8] T. Ito, Formation-flying interferometry in geocentric orbits, Astron. Astrophys. 682 (2024) A38.

[9] J.T. Hansen, M.J. Ireland, A linear formation-flying astronomical interferometer in low earth orbit, Publ. Astron. Soc. Aust. 37 (2020) e019.

[10] T. Matsuo, S. Ikari, H. Kondo, S. Ishiwata, S. Nakasuka, T. Yamamuro, High spatial resolution spectral imaging method for space interferometers and its application to formation flying small satellites, J. Astron. Telesc. Instruments, Syst. 8 (1) (2022) 015001–015001.

[11] D.P. Scharf, F.Y. Hadaegh, Z.H. Rahman, J.F. Shields, G. Singh, M.R. Wette, An overview of the formation and attitude control system for the terrestrial planet finder formation flying interferometer, in: Proceedings from the 2nd International Symposium on Formation Flying Missions and Technologies, 2004.

[12] P.G. Maghami, T.T. Hyde, Laser interferometer space antenna dynamics and controls model, Classical Quantum Gravity 20 (10) (2003) S273.

[13] M. Virdis, S. Vidano, M. Pagone, D. Ruggiero, C. Novara, G. Jonathan, P. Valentin, P. Elisabetta, et al., The LISA DFACS: effects of micrometeoroid impacts in the drag-free mode, in: International Astronautical Congress: IAC Proceedings, International Astronautical Federation, IAF, 2021.

[14] D. Ruggiero, E. Capello, C. Novara, J. Grzymisch, Design of super-twisting sliding mode observer for LISA mission micro-meteoroid impact, in: 2023 American Control Conference, ACC, IEEE, 2023, pp. 4814–4819.

[15] C. Novara, M. Virdis, M. Pagone, D. Ruggiero, E. Capello, E. Punta, S. Dionisio, S. Vidano, J. Grzymisch, V. Preda, Recovery strategies to cope with micrometeoroid impacts in the lisa mission, Acta Astronaut. 211 (2023) 844–864.

[16] Z. Zhao, H. Shang, A. Gao, R. Xu, Autonomous laser-link reacquisition for gravitational wave detection using multistage convex optimization, J. Guid. Control Dyn. 46 (7) (2023) 1348–1364.

[17] S. Gaulocher, C. Pittet, J.-P. Chrétien, Six-DOF formation flying modeling and control with an application to space interferometry, in: Guidance, Navigation and Control Systems, Vol. 606, 2006.

[18] S. Jeon, S.-Y. Park, G.-N. Kim, Relative orbit control algorithms and scenarios for the inertial alignment hold demonstration mission by CubeSat formation flying, Aerosp. 11 (2) (2024) 135.

[19] H. Basu, Y. Pedari, M. Almassalkhi, H.R. Ossareh, Computationally efficient collision-free trajectory planning of satellite swarms under unmodeled orbital perturbations, J. Guid. Control Dyn. 46 (8) (2023) 1548–1563.

[20] C.R. McInnes, Autonomous proximity manoeuvring using artificial potential functions, ESA J. 17 (2) (1993) 159–169.

[21] I. Lopez, C.R. Mclnnes, Autonomous rendezvous using artificial potential function guidance, J. Guid. Control Dyn. 18 (2) (1995) 237–241.

[22] M. Mancini, N. Bloise, E. Capello, E. Punta, Sliding mode control techniques and artificial potential field for dynamic collision avoidance in rendezvous maneuvers, IEEE Control. Syst. Lett. 4 (2) (2019) 313–318.

[23] K. Shahid, P. Gurfil, Guidance for scatter-regather maneuvers of disaggregated satellites, IEEE Trans. Aerosp. Electron. Syst. 50 (4) (2014) 3235–3243.

[24] D. Morgan, G.P. Subramanian, S.-J. Chung, F.Y. Hadaegh, Swarm assignment and trajectory optimization using variable-swarm, distributed auction assignment and sequential convex programming, Int. J. Robot. Res. 35 (10) (2016) 1261–1285.

[25] D. Ruggiero, E. Capello, Model predictive control for spacecraft swarm proximity operations, in: 2023 62nd Annual Conference of the Society of Instrument and Control Engineers, SICE, IEEE, 2023, pp. 894–900.

[26] D. Izzo, L. Pettazzi, Equilibrium shaping: distributed motion planning for satellite swarm, in: Proc. 8th Intern. Symp. on Artificial Intelligence, Robotics and Automation in Space, Vol. 25, 2005.

[27] D. Morgan, S.-J. Chung, F.Y. Hadaegh, Model predictive control of swarms of spacecraft using sequential convex programming, J. Guid. Control Dyn. 37 (6) (2014) 1725–1740.

[28] C.M. Saaj, V. Lappas, V. Gazi, Spacecraft swarm navigation and control using artificial potential field and sliding mode control, in: 2006 IEEE International Conference on Industrial Technology, IEEE, 2006, pp. 2646–2651.

[29] D. Lawrence, E. Frew, W. Pisano, Lyapunov vector fields for autonomous UAV flight control, in: AIAA Guidance, Navigation and Control Conference and Exhibit, 2007, p. 6317.

[30] P. Yao, H. Wang, Z. Su, Real-time path planning of unmanned aerial vehicle for target tracking and obstacle avoidance in complex dynamic environment, Aerosp. Sci. Technol. 47 (2015) 269–279.

[31] D. Celestini, S. Primatesta, E. Capello, Trajectory planning for UAVs based on interfered fluid dynamical system and bézier curves, IEEE Robot. Autom. Lett. 7 (4) (2022) 9620–9626.
[32] J.P. Wilhelm, G. Clem, Vector field UAV guidance for path following and obstacle avoidance with minimal deviation, J. Guid. Control Dyn. 42 (8) (2019) 1848–1856.
[33] Y. Lahana, M. Mancini, D. Peaucelle, E. Capello, H. Evain, Comparison of adaptive control laws on a satellite attitude control benchmark, in: 2023 9th International Conference on Control, Decision and Information Technologies, CoDIT, IEEE, 2023, pp. 1–6.
[34] F. Jiang, J. Li, H. Baoyin, Y. Gao, Study on relative orbit geometry of spacecraft formations in elliptical reference orbits, J. Guid. Control Dyn. 31 (1) (2008) 123–134.
[35] M. Bando, A. Ichikawa, Active formation flying along an elliptic orbit, J. Guid. Control Dyn. 36 (1) (2013) 324–332.
[36] M. Xu, Y. Liang, Formation flying on elliptic orbits by Hamiltonian structure-preserving control, J. Guid. Control Dyn. 41 (1) (2018) 294–300.
[37] M. Bando, A. Ichikawa, Formation flying along halo orbit of circular-restricted three-body problem, J. Guid. Control Dyn. 38 (1) (2015) 123–129.
[38] H. Rouzegar, A. Khosravi, P. Sarhadi, Spacecraft formation flying control around L2 sun-earth libration point using on–off SDRE approach, Adv. Space Res. 67 (7) (2021) 2172–2184.
[39] K. Sugiura, Y. Takao, A.K. Sugihara, Y. Sugawara, O. Mori, Formation flying along artificial halo orbit around sun–earth L2 point for interferometric observations, Acta Astronaut. 208 (2023) 36–48.
[40] W. Clohessy, R. Wiltshire, Terminal guidance system for satellite rendezvous, J. Aerosp. Sci. 27 (9) (1960) 653–658.
[41] W. Fehse, Automated rendezvous and docking of spacecraft, Vol. 16, Cambridge University Press, 2003.
[42] K. Alfriend, S.R. Vadali, P. Gurfil, J. How, L. Breger, Spacecraft Formation Flying: Dynamics, Control and Navigation, Vol. 2, Elsevier, 2009.
[43] J. Tschauner, P. Hempel, Rendezvous zu einem in elliptischer bahn umlaufenden ziel, Astronaut. Acta 11 (2) (1965) 104–+.
[44] T.E. Carter, State transition matrices for terminal rendezvous studies: brief survey and new example, J. Guid. Control Dyn. 21 (1) (1998) 148–155.
[45] K. Yamanaka, F. Ankersen, New state transition matrix for relative motion on an arbitrary elliptical orbit, J. Guid. Control Dyn. 25 (1) (2002) 60–66.
[46] V. Szebehely, Theory Of Orbit: The Restricted Problem of Three Bodies, Elsevier, 2012.
[47] D. Grebow, Generating periodic orbits in the circular restricted three-body problem with applications to lunar south pole coverage, MSAA Thesis, Sch. Aeronaut. Astronaut. Purdue Univ. (2006) 8–14.
[48] G. Franzini, M. Innocenti, Relative motion dynamics in the restricted three-body problem, J. Spacecr. Rockets 56 (5) (2019) 1322–1337.
[49] M. Humi, Planar three-body problem in rendezvous coordinates, J. Guid. Control Dyn. 28 (3) (2005) 553–557.